ELSEVIER

International Journal of Heat and Fluid Flow 21 (2000) 164–175

International Journal of HEAT AND FLUID FLOW

www.elsevier.com/locate/ijhff

Effects of near-wall Reynolds-stress modeling on the calculation of the turbulent thermal field

R.M.C. So *, T.P. Sommer [1], C.Y. Zhao

Department of Mechanical Engineering, Hong Kong Polytechnic University, Hung Hom, Kowloon, Hong Kong, PR China

Received 17 May 1999; accepted 30 November 1999

Abstract

The effects of near-wall Reynolds-stress modeling on the calculation of incompressible wall-bounded turbulent flow with heat transfer were investigated. Two near-wall heat transfer models, a two-equation model and a Reynolds heat flux model, and five different near-wall Reynolds-stress models were considered. All models examined satisfied the wall boundary conditions exactly. Some were asymptotically consistent near the wall, others were not. When the Reynolds-stress models are used in conjunction with the two-equation model to calculate the thermal field, the predicted mean and fluctuating temperature characteristics are found to be essentially the same when the near-wall asymptotes are predicted correctly by the models. However, some discrepancies are noted in a region very near the wall where the calculated dissipation rate of temperature variance differs for the different Reynolds-stress models considered. On the other hand, the calculated mean temperature differs significantly in the outer region when the Reynolds-stress models are used in conjunction with the Reynolds heat flux model and when the near-wall asymptotes are not estimated correctly by the two-equation model. In the former situation, the major source of error can be traced to the modeled equation for the normal heat flux. This equation, in its current modeled form, is very sensitive to the prediction of the leading terms in the near-wall expansions for the turbulent kinetic energy, k, and its dissipation rate, ε. Small differences in these predictions can lead to large discrepancies in the calculations of the normal heat flux in the near-wall region and the mean temperature in the outer region. In the latter situation, the discrepancies can be traced to an incorrect estimate of the near-wall asymptotes of k, ε and the temperature variance and its dissipation rate. This suggests that the temperature field model has to be at least one level lower than the velocity field model. Even then, the models should be able to predict the near-wall asymptotes correctly. © 2000 Elsevier Science Inc. All rights reserved.

Keywords: Turbulent heat flux; Turbulence modelling; Second moment closure

1. Introduction

In the modeling of incompressible turbulent heat transfer, the governing equations are decoupled. That is, the velocity field can influence the calculated temperature field but not the other way around. Consequently, it was pointed out that the model for the temperature field should not be of a higher level than that assumed for the velocity field (Cebeci and Bradshaw, 1984). This meant that if a two-equation model was used to calculate the velocity field, the temperature field could at most be evaluated by a two-equation model. Whether this is also true when Reynolds-stress and Reynolds heat flux models are considered needs to be examined. This point was addressed to a certain extent by the calculations of So et al. (1992). However, they did not systematically investigate the effects of the velocity field model on the calculated thermal field, especially the case involving Reynolds-stress and Reynolds heat flux models.

In the past, heat transfer modeling was invariably carried out using models that were at most of the same level as the velocity field model and wall functions were usually assumed. Even though the effects of different heat transfer models on the calculated temperature field assuming the same velocity field model have been investigated, the influence of the velocity field model on the thermal field calculation was seldom addressed. This is particularly true when it comes to near-wall and second-order modeling of heat transfer problems. In other words, the effect of near-wall Reynolds-stress modeling on the calculated thermal field using a fixed model for the termperature field have not been examined before. For example, if the temperature field model is given by a near-wall Reynolds heat flux model, what is the effect of the near-wall Reynolds-stress model on the calculated thermal field? Further, what is the appropriate heat flux model to use if the velocity field is estimated by a near-wall Reynolds-stress model? The present study attempts to address some of these questions.

* Corresponding author. Tel.: +85-2-2766-6642; fax: +85-2-2364-7183.

E-mail address: mmmcso@hkpucc.polyu.edu.hk (R.M.C. So).

[1] Present address: ABB Power Generation, Gas Turbine Development, CH-5401 Baden, Switzerland

0142-727X/00/$ - see front matter © 2000 Elsevier Science Inc. All rights reserved.
PII: S0142-727X(99)00082-X

Nagano and Shimada (1996) pointed out that even in a relatively simple boundary-layer flow, the heat transfer problem should be investigated using a higher level heat transfer closure scheme, such as a two-equation model. On the other hand, the inadequacy of the two-equation model in the prediction of internal buoyant flows was demonstrated by Sommer and So (1996). Together, these studies provided evidence to support the suggestion that a near-wall Reynolds heat flux model is required if the relatively more complex wall-bounded flows with heat transfer were to be calculated correctly. Lai and So (1990a) developed a near-wall Reynolds heat flux model based on the high-Reynolds-number model suggested by Launder (1978). The model was validated against pipe flow data at Reynolds numbers (Re) around 50,000 using the near-wall Reynolds-stress model of Lai and So (1990b) to calculate the mean ad fluctuating velocity field. Since the heat flux model of Lai and So (1990a) only used the velocity time scale in the model terms, there was no need to calculate the temperature variance, $\overline{\theta^2}$, and its dissipation rate, ε_θ, at least for flows with no buoyancy effects. This is not so for buoyant flows because equations for $\overline{\theta^2}$ and ε_θ have to be solved also. Therefore, this Reynolds heat flux model could be fairly attractive, especially for flows that change only in one or two space dimensions. For incompressible flows, only one or two heat flux equations need to be solved, versus two for any near-wall two-equation model for the heat fluxes, such as that proposed by Sommer et al. (1992). Even in three dimensions, the number of equations would not become excessive. However, the only drawback is the necessity to use a Reynolds-stress model for the velocity field (Cebeci and Bradshaw, 1984).

When the near-wall Reynolds heat flux model (Lai and So, 1990a) was used with the near-wall Reynolds-stress model of Lai and So (1990b) to predict channel and pipe flows with heat transfer, good agreement with measurements were obtained. However, its performance with other near-wall Reynolds-stress models is not known. In the past, when wall functions were assumed, once a Reynolds heat flux model was shown to work well with a particular high-Re Reynolds-stress model, its suitability with other similar models was taken for granted. The hypothesis was seldom tested. The reason was that the near-wall turbulence field, which was assumed to be local equilibrium turbulence, was taken to be the same for all Reynolds-stress models. With the advent of near-wall models, the near-wall behavior is calculated and the predicted turbulence statistics could vary from model to model. The normal heat flux is very sensitive to the calculated normal stress $\overline{v^2}$. Therefore, it is conceivable that near-wall Reynolds-stress models could affect the calculated thermal field if a Reynolds heat flux model is used. The same may not be true for two-equation or lower level heat-flux models, where the normal heat flux is obtained by invoking the gradient transport assumption and an eddy thermal diffusivity, α_t. This α_t can be isotropic or anisotropic and can depend on $k, \varepsilon, \overline{\theta^2}$ and ε_θ, the turbulent kinetic energy and its dissipation rate, the temperature variance and its dissipation rate, respectively (Sommer et al., 1992; So and Sommer, 1994, 1996).

The effect of Reynolds-stress modeling on the calculated thermal field could be investigated by choosing a particular two-equation or Reynolds heat flux model and using different Reynolds-stress models to determine the velocity field. For incompressible heat transfer problems, the temperature field is influenced by the calculated velocity field but not the other way around. Therefore, these kinds of heat transfer problems are ideal candidates for the assessment of Reynolds-stress modeling effects. Once a heat flux model has been identified, the choice of Reynolds-stress models needs some consideration. The performance of different near-wall Reynolds-stress models has been examined by So et al. (1991) and reviewed by Speziale and So (1998). These near-wall models range from the relatively simple proposal of Hanjalic and Launder (1976) to that of Launder and Tselepidakis (1993), where the fully realizable condition was satisfied. All these models assume the high-Re Kolmogorov (1941) model for the dissipation rate tensor, ε_{ij}, and either the model of Daly and Harlow (1970), that of Hanjalic and Launder (1972) or that of Shir (1973) for the turbulent diffusion tensor, D^t_{ij}. As for the velocity-pressure-gradient correlation tensor, Π_{ij}, most adopted the models of Launder et al. (1975) and Speziale et al. (1991) for the pressure strain part of Π_{ij}, and neglected the pressure diffusion part of Π_{ij}. Some closures even generalized the Launder et al. (1975) model to include cubic terms in the rapid part of Π_{ij} (Launder and Tselepidakis, 1993). The near-wall corrections vary from simple terms, which are qualified by a viscous damping function, added to either ε_{ij} or Π_{ij} to render the modeled equations regular at the wall (Shima, 1988) to modifying the coefficients of the Π_{ij} model to satisfy the wall boundary conditions (Launder and Shima, 1989). Other approaches vary from the requirements that the near-wall asymptotes of the turbulence quantities have to be recovered exactly from the modeled equations (Lai and So, 1990b; Zhang et al., 1993; So and Yuan, 1999) to a careful analysis of the viscous-like pressure-diffusion process near a wall (Launder and Tselepidakis, 1993). This latter approach led to a near-wall model to account for the pressure diffusion part of Π_{ij}.

In view of the fact that most of the near-wall Reynolds-stress models are derived based on two different Π_{ij} proposals, the choice of near-wall models should at least consider these two different types of Π_{ij}. Furthermore, the choice should also include simple as well as more complicated models for Π_{ij}, such as whether wall reflection terms are included to account for the pressure blocking effects due to the presence of a wall. Another criterion is the proposed corrections for the near-wall flow, whether they depend on the wall unit normals and the wall normal coordinate. Therefore, the choice of models should also include those that have different near-wall corrections in the Π_{ij} and ε_{ij} models and in the ε-equation.

Based on these criteria, the effects of Reynolds-stress modeling could be investigated by carrying out calculations using the near-wall models of Lai and So (1990b), Zhang et al. (1993), Hanjalic and Launder (1976), Launder and Shima (1989) and So et al. (1996). For the sake of brevity, these models are designated as LS, ZSZ, HL, LSH and SAYS, respectively. The first four closures invoked variations of the Launder et al. (1975) model for the pressure strain part of Π_{ij}, while the last closure assumed the Speziale et al. (1991) model instead. Of the five models, two (LSH and ZSZ) adopt the pressure strain models that used wall reflection terms to account for the pressure blocking effects; the other three (HL, LS and SAYS) do not. Two of these five (LS and ZSZ) have identical high-Re models, but only differ in the near-wall corrections proposed. The assumption of different pressure strain models leads to various near-wall corrections and hence different models for the viscous dissipation rate tensor. Furthermore, the dissipation rate equation solved also differs from one closure to another. Finally, among the five models considered, one (HL) is geometry independent, i.e. the models only depend on local properties. The other four are not because their models have dependence on the wall unit normal and the wall normal coordinate. This choice of near-wall Reynolds-stress models is by no means unique or comprehensive. It does offer an assessment of the effects of Reynolds-stress modeling due to near-wall corrections, to different Π_{ij} models, to the ε-equation and to the wall unit normals.

Together, these five Reynolds-stress models offered sufficient differences between them to test the effects of the calcu-

lated velocity field on the thermal field predicted by a near-wall Reynolds heat flux model. In order to further investigate the effects of Reynolds-stress modeling on the calculated mean temperature field when the heat flux model is at least one level lower, the five Reynolds-stress models and a near-wall two-equation heat flux model are also used to calculate identical incompressible heat transfer problems for comparison. The discrepancies or lack thereof between the model calculations are examined. An attempt is then made to analyze the discrepancies in the calculated mean temperature and to show that it is consistent with the errors observed in the prediction of the normal heat flux. It is further demonstrated, by means of asymptotic expansion in terms of $y^+ = yu_\tau/\nu$, where y is the normal coordinate, ν the fluid kinematic viscosity and u_τ is the friction velocity, that an error in the leading term of the solution of the relevant equations could lead to an even larger error in the second term in the expansions. Thus, errors could propagate and amplify to give the discrepancy observed in the prediction of the mean temperature given by the the Reynolds-stress models. Finally, an alternative to the Reynolds heat flux model is suggested. The proposed model would yield similar heat flux predictions as the Reynolds heat flux model.

2. Turbulent heat flux models

Details of the development of the near-wall Reynolds heat flux model are given in Lai and So (1990a). Here, only points relevant to this study are discussed. The exact equations for the turbulent heat fluxes can be written out fully and symbolically (Launder, 1978) as:

$$\frac{\mathrm{D}\overline{u}_i\theta}{\mathrm{D}t} = \frac{\partial}{\partial x_j}\left[\nu\theta\overline{\frac{\partial u_i}{\partial x_j}} + \alpha u_i\overline{\frac{\partial\theta}{\partial x_j}}\right] - \frac{\partial}{\partial x_j}\left[\overline{u_iu_j\theta} + \overline{\frac{p\theta}{\rho}}\delta_{ij}\right] + \left[-\overline{u_iu_j}\frac{\partial\Theta}{\partial x_j} - \overline{u_j\theta}\frac{\partial U_i}{\partial x_j}\right] + \overline{\frac{p}{\rho}\frac{\partial\theta}{\partial x_i}} - (\alpha+\nu)\overline{\frac{\partial\theta}{\partial x_k}\frac{\partial u_i}{\partial x_k}}, \tag{1a}$$

$$C_{i\theta} = D^{\nu}_{i\theta} + D^{\mathrm{t}}_{i\theta} + P_{i\theta} + \Phi_{i\theta} - \varepsilon_{i\theta}, \tag{1b}$$

where U_i and u_i are the Reynolds mean and fluctuating velocity vector, Θ and θ the mean and fluctuating temperatures, p the fluctuating pressure, ρ the fluid density, α the molecular thermal diffusivity, t the time and x_i is the ith component of the coordinate. In (1a) and (1b), the terms represent, from left to right, convection, molecular transport, turbulent diffusion, production due to mean temperature gradient and mean shear, pressure-scrambling and destruction of the heat fluxes. All terms in (1a) and (1b), except the convection and production of heat fluxes, need modeling. At high Re, the molecular transport terms can be neglected. Also, the dissipation term is zero for isotropic turbulence. For anisotropic turbulence, the dissipation term can also be neglected provided Re is high (Launder, 1978). The model terms proposed by Launder (1978) for this case and adopted by Lai and So (1990a) are:

$$D^{\mathrm{t}}_{i\theta} = \frac{\partial}{\partial x_j}\left\{C_{s\theta}\frac{k}{\varepsilon}\left[\overline{u_iu_k}\frac{\partial\overline{u_j\theta}}{\partial x_k} + \overline{u_ju_k}\frac{\partial\overline{u_i\theta}}{\partial x_k}\right]\right\}, \tag{2}$$

$$\Phi_{i\theta} = -C_{1\theta}\frac{\varepsilon}{k}\overline{u_i\theta} + C_{2\theta}\overline{u_k\theta}\frac{\partial U_i}{\partial x_k}, \tag{3}$$

where $C_{s\theta}, C_{1\theta}$ and $C_{2\theta}$ are model constants. With the introduction of two modeled terms and a set of properly chosen constants, the high-Re model is complete. Lai and So (1990a) adopted $C_{s\theta} = 0.11, C_{1\theta} = 3$ and $C_{2\theta} = 0.4$, which lie within the range reported by Launder (1978). Note that only the velocity time scale is used in (3), although Launder (1978) suggested that both velocity and thermal time scales should be included for more general applications. The reason was that the inclusion of the thermal time scale necessitated solving the $\overline{\theta^2}$ and ε_θ equations, which were not required for the solution of the incompressible heat flux equation.

Having settled on an appropriate high-Re model, Lai and So (1990a) proceeded to develop a near-wall correction to this model. It involved adding model terms for the molecular transport and the dissipation, because the viscous terms in (1a) were not of the right form. These terms were derived with the help of asymptotic expansions for the turbulent quantities. The terms were determined to give the proper near-wall behavior compared to the exact equations. Details are given in Lai and So (1990b). Here, only the final result is given,

$$\begin{aligned}\frac{\mathrm{D}\overline{u_i\theta}}{\mathrm{D}t} = {} & \frac{\partial}{\partial x_j}\left[\nu\frac{\partial\overline{u_i\theta}}{\partial x_j} + \frac{\alpha-\nu}{n_i+2}\frac{\partial\overline{u_i\theta}}{\partial x_j}\right] + \frac{\partial}{\partial x_j}\left\{C_{s\theta}\frac{k}{\varepsilon}\left[\overline{u_iu_k}\frac{\partial\overline{u_j\theta}}{\partial x_k} + \overline{u_ju_k}\frac{\partial\overline{u_i\theta}}{\partial x_k}\right]\right\} - \overline{u_iu_j}\frac{\partial\Theta}{\partial x_j} - \overline{u_j\theta}\frac{\partial U_i}{\partial x_j} - C_{1\theta}\frac{\varepsilon}{k}\overline{u_i\theta} \\ & + C_{2\theta}\overline{u_j\theta}\frac{\partial U_i}{\partial x_j} + f_{w\theta}\left[C_{1\theta}\frac{\varepsilon}{k}\overline{u_i\theta} - \frac{\varepsilon}{k}\overline{u_k\theta}n_kn_i\right] \\ & - \frac{1}{2}f_{w\theta}\left[1+\frac{1}{Pr}\right]\frac{\varepsilon}{k}\left(\overline{u_i\theta} + \overline{u_k\theta}n_kn_i\right),\end{aligned} \tag{4}$$

where Pr is the molecular Prandtl number, n_i the unit vector measured positive from the wall, $f_{w\theta} = \exp[-(Re_{\mathrm{t}}/80)^2]$ is the near-wall damping function and $Re_{\mathrm{t}} = k^2/\varepsilon\nu$.

A similar procedure has been used by Sommer et al. (1992) to derive a near-wall two-equation model for the heat fluxes. In this model, the gradient transport assumption was invoked and α_{t} was assumed to be isotropic. Since the transport equations for θ^2 and ε_θ are solved, it was possible to adopt a mixed time scale for the definition of α_{t}. The model had also been modified for flows with widely different Pr (So and Sommer, 1994). Since details are available in So and Sommer (1996), only the modeled equations for θ^2 and ε_θ are given here,

$$\frac{\mathrm{D}\overline{\theta^2}}{\mathrm{D}t} = \frac{\partial}{\partial x_j}\left[\alpha\frac{\partial\overline{\theta^2}}{\partial x_j}\right] + \frac{\partial}{\partial x_k}\left[C_{\theta^2}\frac{k}{\varepsilon}\overline{u_ku_j}\frac{\partial\overline{\theta^2}}{\partial x_j}\right] - 2\overline{u_j\theta}\frac{\partial\Theta}{\partial x_j} - 2\varepsilon_\theta, \tag{5}$$

$$\frac{\mathrm{D}\varepsilon_\theta}{\mathrm{D}t} = \frac{\partial}{\partial x_j}\left[\alpha\frac{\partial\varepsilon_\theta}{\partial x_j}\right] + \frac{\partial}{\partial x_k}\left[C_{\varepsilon_\theta}\frac{k}{\varepsilon}\overline{u_ku_j}\frac{\partial\varepsilon_\theta}{\partial x_j}\right] + C_{d1}\frac{\varepsilon_\theta}{\overline{\theta^2}}P_\theta + C_{d2}\frac{\varepsilon}{k}P_\theta + C_{d3}\frac{\varepsilon_\theta}{k}\tilde{P} - C_{d4}\frac{\tilde{\varepsilon}_\theta}{\overline{\theta^2}}\varepsilon_\theta - C_{d5}\frac{\tilde{\varepsilon}}{k}\varepsilon_\theta + \xi_{\varepsilon_\theta}, \tag{6}$$

$$\xi_{\varepsilon_\theta} = f_{w,\varepsilon_\theta}\left[(C_{d4}-4)\frac{\tilde{\varepsilon}_\theta}{\overline{\theta^2}}\varepsilon_\theta + C_{d5}\frac{\tilde{\varepsilon}}{k}\varepsilon_\theta - \frac{\varepsilon_\theta^{*2}}{\overline{\theta^2}} + (2 - C_{d1} - PrC_{d2})\frac{\varepsilon_\theta}{\overline{\theta^2}}P^*_\theta\right], \tag{7}$$

$$-\overline{u_i\theta} = \alpha_{\mathrm{t}}\frac{\partial\Theta}{\partial x_i}, \tag{8}$$

$$\alpha_{\mathrm{t}} = c_\lambda f_\lambda k\left[\frac{k}{\varepsilon}\frac{\overline{\theta^2}}{\varepsilon_\theta}\right]^{1/2}, \tag{9}$$

$$f_\lambda = (1 - f_{\lambda 1})\frac{C_{\lambda 1}}{Re_{\mathrm{t}}^{1/4}} + f_{\lambda 1}, \tag{10}$$

where $P_\theta = -\overline{u_k\theta}(\partial\Theta/\partial x_k)$, P_θ^* is the production of temperature variance due to the streamwise temperature gradient alone, $\tilde{P} = P_{ii}/2 = -\overline{u_iu_k}(\partial U_i/\partial x_k)$ is the production of $k, f_{w,\varepsilon_\theta} = f_{w\theta}, \tilde{\varepsilon} = \varepsilon - 2\nu(\partial\sqrt{k}/\partial y)^2, \tilde{\varepsilon}_\theta = \varepsilon_\theta - \alpha(\partial\sqrt{\overline{\theta^2}}/\partial y)^2, \varepsilon_\theta^* = \varepsilon_\theta - 2\alpha(\overline{\theta^2}/y^2)$, $f_{\lambda1} = [1-\exp(-y^+/A^+)]^2$ and $C_{\lambda1}$ and A^+ are model constants parametric in Pr. The model constants are specified as: $C_{d1} = 1.80, C_{d2} = 0,\ C_{d3} = 0.72, C_{d4} = 2.20, C_{d5} = 0.80, C_{\theta^2} = 0.11$, $C_{\varepsilon_\theta} = 0.11, c_\lambda = 0.095, C_{\lambda1} = 0.4/Pr^{1/4}$ for $Pr < 0.1$, $C_{\lambda1} = 0.07/Pr$ for $Pr \geqslant 0.1, A^+ = 10/Pr$ for $Pr < 0.25$ and $A^+ = 39/Pr^{1/16}$ for $Pr \geqslant 0.25$.

The wall boundary conditions for Eqs. (4)–(6) are the no-slip condition, $\overline{u_i\theta} = 0$, the assumption $\overline{\theta^2} = 0$ and $\varepsilon_\theta = (\varepsilon_\theta)_w = \alpha(\partial\sqrt{\overline{\theta^2}}/\partial y)^2$. Strictly speaking, temperature variance cannot vanish at the wall because it implies a zero wall fluctuating pressure for incompresssible flows. In practice, the assumption has little or no effect on the predicted integral properties (Sommer et al., 1994). The only effect it has is in the prediction of $\overline{\theta^2}$ and ε_θ in a region very close to the wall. Therefore, the assumption $\overline{\theta^2} = 0$ at the wall is justified.

3. Reynolds-stress models

The LS and ZSZ near-wall Reynolds-stress models invoke common high-Re models for D_{ij}^t, Π_{ij} and ε_{ij}, and solve an identical high-Re ε-equation. Their differences are in the near-wall corrections proposed for the Π_{ij} model and the ε-equation. The modeled equations can be written in Cartesian tensor form as:

$$\frac{\mathrm{D}\overline{u_iu_j}}{\mathrm{D}t} = \frac{\partial}{\partial x_k}\left[\nu\frac{\partial\overline{u_iu_j}}{\partial x_k}\right] + D_{ij}^t + P_{ij} + \Pi_{ij} - \varepsilon_{ij}, \tag{11}$$

$$\frac{\mathrm{D}\varepsilon}{\mathrm{D}t} = \frac{\partial}{\partial x_k}\left[\nu\frac{\partial\varepsilon}{\partial x_k}\right] + \frac{\partial}{\partial x_k}\left[C_\varepsilon\frac{k}{\varepsilon}\overline{u_iu_k}\frac{\partial\varepsilon}{\partial x_i}\right] + C_{\varepsilon1}\frac{\varepsilon}{k}\tilde{P} - C_{\varepsilon2}\frac{\tilde{\varepsilon}}{k}\varepsilon + \xi, \tag{12}$$

$$D_{ij}^t = \frac{\partial}{\partial x_k}\left\{C_s\frac{k}{\varepsilon}\left[\overline{u_iu_l}\frac{\partial\overline{u_ju_k}}{\partial x_l} + \overline{u_ju_l}\frac{\partial\overline{u_ku_i}}{\partial x_l} + \overline{u_ku_l}\frac{\partial\overline{u_iu_j}}{\partial x_l}\right]\right\}, \tag{13}$$

$$\varepsilon_{ij} = \frac{2}{3}(1-f_{w1})\varepsilon\delta_{ij} + f_{w1}\frac{\epsilon}{k} \times \frac{\overline{u_iu_j} + \overline{u_iu_k}n_kn_j + \overline{u_ju_k}n_kn_i + n_in_j\overline{u_ku_l}n_kn_l}{1 + 3\overline{u_ku_i}n_kn_l/2k}, \tag{14}$$

while the models for Π_{ij} can be written in a common form as:

$$\begin{aligned}\Pi_{ij} = &-C_1(1-f_{w1})\frac{\varepsilon}{k}\left[\overline{u_iu_j} - \frac{2}{3}k\delta_{ij}\right] - (\alpha_1 - \alpha^* f_{w1})\left[P_{ij} - \tilde{P}\delta_{ij}\right] \\ &- \beta_1\left[D_{ij} - \tilde{P}\delta_{ij}\right] - 2\left[\gamma_1 - C_w\frac{k^{3/2}}{\varepsilon y}\right]kS_{ij} \\ &- f_{w1}\frac{\varepsilon}{k}[\overline{u_iu_k}n_kn_j + \overline{u_ju_k}n_kn_i].\end{aligned} \tag{15}$$

Here,

$$\begin{aligned}D_{ij} &= -\overline{u_iu_k}(\partial U_k/\partial x_j) - \overline{u_ju_k}(\partial U_k/\partial x_i), \\ P_{ij} &= -\overline{u_iu_k}(\partial U_j/\partial x_k) - \overline{u_ju_k}(\partial U_i/\partial x_k), \\ S_{ij} &= (1/2)[\partial U_i/\partial x_j + \partial U_j/\partial x_i]\end{aligned}$$

and the damping function is $f_{w1} = \exp[-(Re_t/A)^2]$. The two models adopt different values for C_w to account for wall reflection effects. As a result of this difference, the near-wall correction ξ for the ε-equation also differs. Based on an asymptotic analysis, the near-wall corrections thus deduced are:

$$\xi = f_{w2}\left[\left(\frac{7}{9}C_{\varepsilon2} - 2\right)\frac{\varepsilon\tilde{\varepsilon}}{k} - \frac{1}{2}\frac{\bar{\varepsilon}^2}{k}\right], \tag{16}$$

$$\xi = f_{w2}\left[1.5\frac{\bar{\varepsilon}^2}{k} - 2\frac{\varepsilon\tilde{\varepsilon}}{k} - 1.5C_{\varepsilon1}\tilde{P}\right], \tag{17}$$

for the LS and ZSZ model, respectively. Here, $\tilde{\varepsilon}$ and $\bar{\varepsilon} = \varepsilon - 2\nu k/y^2$ are reduced ε introduced to render the ε-equation regular as a will is approached and the damping function is defined as $f_{w2} = \exp[-(Re_t/40)^2]$.

The differences between these two near-wall models are in the modeling of Π_{ij} and ξ. Near-wall corrections including wall reflection effects (Launder et al., 1975) are present in the ZSZ model and they introduce $C_w = -0.00805 + 0.00519\ \log(Re)$ for pipe and channel flows. On the other hand, C_w is set to zero in the LS model. Therefore, one model takes wall reflection effects into account while the other does not. The model constants $A, C_1, C_2, \alpha_1, \beta_1, \gamma_1, \alpha^*, C_s, C_\varepsilon, C_{\varepsilon1}, C_{\varepsilon2}$ are set equal to 150, 1.5, 0.4, 0.7636, 0.1091, 0.1818, 0.45, 0.11, 0.15, 1.35, 1.80 for the LS model, and to 150, 1.5, 0.4, 0.7636, 0.1091, 0.1818, 0.45, 0.11, 0.10, 1.50, 1.83 for ZSZ model. Finally, the wall boundary conditions for the turbulent velocity field are given by $\overline{u_iu_j} = 0$ and $\varepsilon_w = 2\nu(\partial\sqrt{k}/\partial y)^2$.

The equations of the HL model can be cast into a form similar to (11)–(15). There are minor difference in (12), (14) and (15) though. In the case of (15), the constants and the damping functions take on the values $C_1 = 1.5$, $\alpha_1 = 0.7636$, $\beta_1 = 0.1091$, $\gamma_1 = 0.1818$, $C_w = 0$ and $f_{w1} = 0$. As for (14), the model adopted for ε_{ij} is given by

$$\varepsilon ij = \frac{2}{3}\varepsilon\left\{(1-f_s)\delta_{ij} + \frac{\overline{u_iu_j}}{2k/3}f_s\right\}, \tag{18}$$

where $f_s = (1 + Re_t/10)^{-1}$ is the assumed damping function. This choice of near-wall correction is based on the arguments that, to the lowest order, ν does not appear in Π_{ij} and therefore Π_{ij} does not need to be modified to account for viscous effects. Furthermore, very near the wall, the energy-containing and the dissipative range of motions overlap (Rotta, 1951) and ε_{ij} could be approximated by $\varepsilon_{ij} = \overline{u_iu_j}(\varepsilon/k)$. Note the absence of n_i and wall normal coordinate in this model. Therefore, this model is geometry independent.

The differences between the ε-equation solved in the HL model and (12) are in the choice of model constants, the destructive term, $C_{\varepsilon2}(\tilde{\varepsilon}/k)\varepsilon$, and ξ. The function

$$\xi = C_{\varepsilon3}\nu\frac{k\overline{u_ju_k}}{\varepsilon}\left(\frac{\partial^2U_i}{\partial x_j\partial x_l}\right)\left(\frac{\partial^2U_i}{\partial x_k\partial x_l}\right) \tag{19}$$

is invoked with the model constants associated with (12) and (34) specified as $C_\varepsilon = 0.15$, $C_{\varepsilon1}, = C_{\varepsilon2} - 3.5C_\varepsilon = 1.275$, $C_{\varepsilon2} = 1.80$ and $C_{\varepsilon3} = 2.0$. An additional damping function was introduced into the destructive term so that the term now reads $C_{\varepsilon2}f_\varepsilon(\tilde{\varepsilon}/k)\varepsilon$, where f_ε is defined as $f_\varepsilon = 1 - (2/9)\exp[-(Re_t/6)^2]$.

The major differences between the modeled equations of LSH model and those given in (11)–(15) are in the modeling of ε_{ij} and Π_{ij}, and in the choice of coefficients in the ε-equation. First of all, (14) is replaced by the conventional Kolmogorov model while the anisotropic behavior of the small scale trubulence is accounted for in the modeling of Π_{ij}. As a result, Π_{ij} is modeled by splitting it into four parts, namely,

$$\Pi_{ij} = \Pi_{ij1} + \Pi_{ij2} + \Pi_{ij1}^w + \Pi_{ij2}^w, \tag{20}$$

where Π_{ij1} and Π_{ij2} are given by the first and second term in (15), respectively, with $f_{w1} = 0$ specified. The models for Π_{ij1}^w and Π_{ij2}^w are formulated to be:

$$\Pi^w_{ij1} = C^w_1 \frac{\varepsilon}{k}\left[\overline{u_k u_m} n_k n_m \delta_{ij} - \frac{3}{2}\overline{u_k u_i} n_k n_j - \frac{3}{2}\overline{u_k u_j} n_k n_i\right] f, \tag{21a}$$

$$\Pi^w_{ij2} = C^w_2 \frac{\varepsilon}{k}\left[\Pi_{km2} n_k n_m \delta_{ij} - \frac{3}{2}\Pi_{ik2} n_k n_j - \frac{3}{2}\Pi_{jk2} n_k n_i\right] f, \tag{21b}$$

where the damping function f is given by $f = 0.4k^{3/2}/\varepsilon y$ and the model constants are specified as:

$$C_1 = 1 + 2.58AA_2^{1/4}\{1 - \exp[-(0.0067Re_t)^2]\}, \tag{22a}$$

$$\alpha_1 = 0.75A^{1/2}, \tag{22b}$$

$$C^w_1 = -\frac{2}{3}C_1 + 1.67, \tag{22c}$$

$$C^w_2 = \max\left[\left(\frac{2}{3}C_2 - \frac{1}{6}\right)\Big/ C_2, 0\right]. \tag{22d}$$

Here, $A = [1 - (9/8)(A_2 - A_3)], A_2 = a_{ik}a_{ki}, A_3 = a_{ik}a_{kj}a_{ji}$ and $a_{ij} = [\overline{u_i u_j} - (2/3)k\delta_{ij}]/k$. The ε-equation used is similar to (12) but the coefficient $C_{\varepsilon 1}$ is modified to give $(C_{\varepsilon 1} + \psi_1 + \psi_2)$ with $\psi_1 = 2.5A(\tilde{P}/\varepsilon - 1)$ and $\psi_2 = 0.3(1 - 0.3A_2)\exp[-(0.002Re_t)^2]$ specified. Thus modified, the constants are given by $C_\varepsilon = 0.18, C_{\varepsilon 1} = 1.45$ and $C_{\varepsilon 2} = 1.90$.

The differences between the SAYS and the other four models are in Π_{ij} and ξ. All other model terms are identical to those given (11)–(14). The modeled Π_{ij} and ξ terms are:

$$\begin{aligned}\Pi_{ij} = &-(2C_1\varepsilon + C^*_1\tilde{P})(1 - f_{w1})b_{ij} + C_2(1 - f_{w1})\varepsilon\left(b_{ik}b_{kj} - \frac{1}{3}\Pi\delta_{ij}\right)\\ &-(\alpha - \alpha^* f_{w1})(P_{ij} - \tilde{P}\delta_{ij}) - \beta_1(D_{ij} - \tilde{P}\delta_{ij})\\ &-2\left(\gamma_1 - f_{w1}\gamma^* + \frac{C^*_3}{2}\Pi^{1/2}\right)kS_{ij}\\ &-\frac{1}{3}\left[\frac{\partial}{\partial x_m}\left(v\frac{\partial\overline{u_i u_k}}{\partial x_m}\right)n_k n_j + \frac{\partial}{\partial x_m}\left(v\frac{\partial\overline{u_j u_k}}{\partial x_m}\right)n_k n_i\right]\\ &+\frac{1}{3}\frac{\partial}{\partial x_m}\left(v\frac{\partial\overline{u_k u_p}}{\partial x_m}\right)n_k n_p n_i n_j,\end{aligned} \tag{23}$$

$$\xi = f_{w2}\left[-2.25\frac{\varepsilon}{k}\tilde{P} + 0.5\frac{\overline{\varepsilon}^2}{k} - 0.57\frac{\varepsilon\tilde{\varepsilon}}{k}\right], \tag{24}$$

where $b_{ij} = a_{ij}/2$ and $\Pi = b_{ij}b_{ij}$. The damping function f_{w1} and f_{w2} are taken to be the same as those defined for the LS and ZSZ model, and the constants $A, C_1, C_2, C^*_1, C^*_3, \alpha_1, \beta_1, \gamma_1, \alpha^*, \gamma^*, C_s, C_\varepsilon, C_{\varepsilon 1}, C_{\varepsilon 2}$ are set equal to 200, 1.7, 4.2, 1.8, 1.3, 0.4125, 0.2125, −0.29, 0.0167, 0.065, 0.11, 0.11, 1.50, 1.83, respectively.

4. Turbulent thermal field calculations

Turbulent pipe and channel flow calculations are carried out using the above models. The mean flow equations of fully developed pipe and channel flows are particularly simple and can be reduced to ordinary differential equations. Furthermore, the model Reynolds turbulence equations can also be reduced to ordinary differential equations. This means that the governing equations can be solved using standard numerical techniques and the estimated errors involved are relatively small and known. Therefore, comparisons can be made on a common basis and the calculated discrepancies between different models could be attributed to model performance. The mean flow equations, the numerical technique employed and the numerical errors are given in Lai and So (1990b). It is sufficient to point out that the same numerical method is adopted in the present study.

It is obvious that the LS and ZSZ models only differ in the modeling of the near-wall effects; one models wall reflection while the other does not. Therefore, it will be interesting to first examine the effects of these two Reynolds-stress models on the calculated temperature field. The first step is to assess the effects of the Reynolds-stress models on the thermal field using a two-equation heat flux model. For these calculations, the equations solved are given by (5)–(17) plus the mean flow equations. Kader (1981) has collected a wide range of data on fully developed pipe flow with heat transfer and has proposed an empirical relation for $\Theta^+ = \Theta/\Theta_t$ versus y^+ that is parametric in Pr and the pipe Reynolds number, $Re = U_m 2R/v$. Here, Θ_τ is the friction temperature, U_m the bulk mean velocity and R is the pipe radius. The calculations were carried out for the case where $Re = 40,000$ and $Pr = 0.71$ and the results are compared in Figs. 1–5. The mean volecities U are compared by plotting $U^+ = U/u_t$ versus y^+ (Fig. 1). The log law with an intercept of 5.5 is also shown for comparison.

It can be seen that the ZSZ model yields a mean velocity that agrees with the log law, but this is not true for the LS model. In the near-wall region, the two model predictions are in agreement. The agreement does not seem to extend to the near-wall asymptote, $k^+/\varepsilon^+ y^{+2}$, though. According to asymptotic analysis, this value should be exactly 0.5 (So et al., 1991). A value of 0.48 is predicted by the LS model while the ZSZ model yields 0.5. This is perhaps the reason why the LS model gives a U^+ that has a maximum error of about 10% at the pipe center. In spite of this difference, the predicted Θ^+ profiles are essentially identical (Fig. 2) and are in agreement with the data of Kader (1981). An examination of (9) reveals that α_t depends on k and the ratios k/ε and $\overline{\theta^2}/\varepsilon_\theta$. If these parameters are

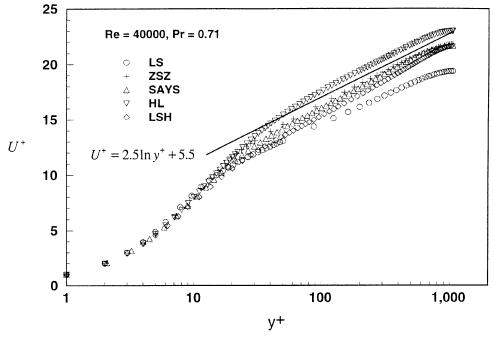

Fig. 1. Comparisons U^+ calculations using different Reynolds-stress models with the log law.

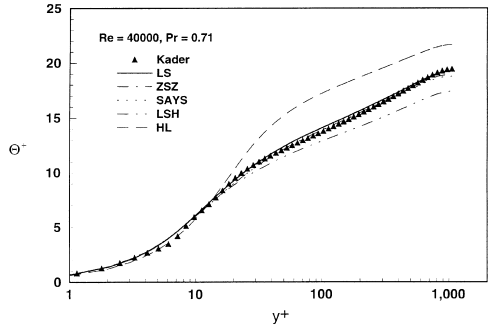

Fig. 2. Θ^+ calculations using a two-equation model for the temperature field and different Reynolds-stress models.

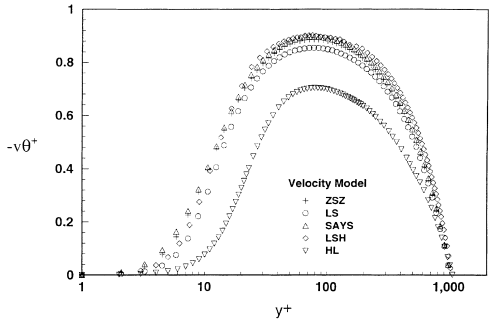

Fig. 3. $v\theta^+$ calculations using a two-equation model for the temperature field and different Reynolds-stress models.

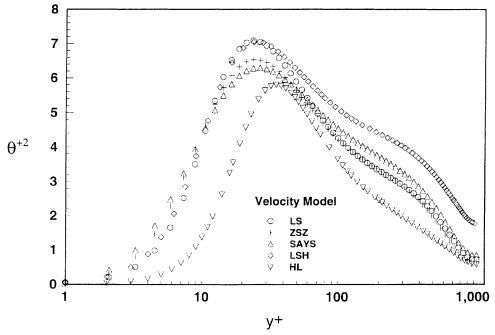

Fig. 4. θ^{+2} calculations using a two-equation model for the temperature field and different Reynolds-stress models.

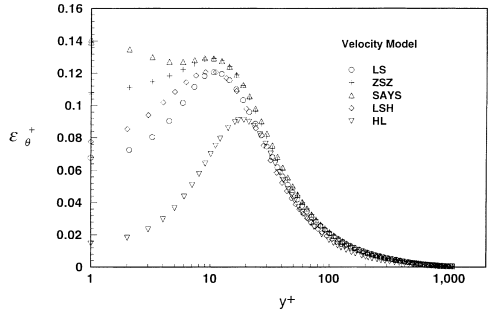

Fig. 5. ε_θ^+ calculations using a two-equation model for the temperature field and different Reynolds-stress models.

calculated correctly in the near-wall region, the likelihood that Θ^+ could be calculated correctly is much higher. The two-equation heat flux model yields the correct asymptote for $\theta^{+2}/\varepsilon_\theta^+ y^{+2}$, which is Pr (Sommer et al., 1992). Here, $\theta^{+2} = \overline{\theta^2}/\Theta_\tau^2$ and $\varepsilon_\theta^+ = \varepsilon_\theta \nu/(u_\tau^2 \Theta_\tau^2)$. Therefore, in spite of the fact that the LS and ZSZ models yield slightly different asymptotes for $k^+/\varepsilon^+ y^{+2}$ and k^+, the overall estimate of α_t is essentially correct. Consequently, both models give the same predictions for Θ^+.

Good correlation in Θ^+ also translates to a similarly good agreement in the calculated normal heat flux, $v\theta^+ = \overline{v\theta}/u_\tau \Theta_\tau$ Fig. 3. Here, slight differences between model calculations are noted in the near-wall region and in the region surrounding the maximum heat flux. A similar behavior is also observed in the comparisons of the calculated θ^{+2} (Fig. 4) and ε_θ^+ (Fig. 5). The near-wall Reynolds-stress model contributes to the difference observed in ε_θ^+ in the vicinity of the wall. Beyond $y^+ = 20$, the

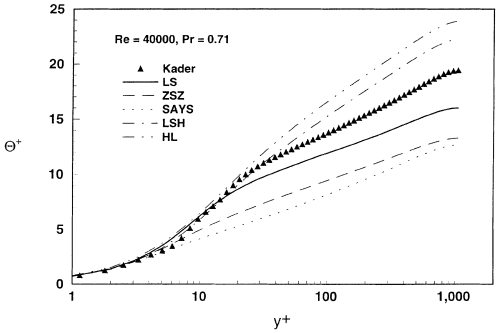

Fig. 6. Comparisons of Θ^+ calculations using a Reynolds heat flux model and three different Reynolds-stress models with data.

calculations are essentially identical. However, the ε_θ^+ difference in the near-wall region does not seem to affect the predictions of other thermal properties. Calculations of other pipe and channel flow with different Re and Pr show similar behavior. Therefore, these results show that the LS and ZSZ models have little effect on the calculated thermal field when a near-wall two-equation heat flux model, which is one level lower than the Reynolds-stress model, is used.

Eqs. (1a), (1b), (2)–(4) and (11)–(17) are solved next for the same fully developed pipe flow case. These calculations represent near-wall Reynolds-stress and Reynolds heat flux modeling of the flow. The only difference between this set of calculations and the previous set is in the heat flux model adopted. For an incompressible flow, the velocity field results are not affected by the heat flux calculations, while the thermal field is influenced by the velocity field. Therefore, the same mean velocities as those shown in Fig. 1 are obtained. The mean temperature comparisons are shown in Fig. 6. Three observations can be made from this result. First, the best correlation is given by the LS model which yields the worse result for the mean velocity. The second is that error as large as 34% is observed at the pipe centerline and the model calculations, in general, do not agree with the data of Kader (1981). Finally, in spite of the fact that LS and ZSZ models use the same high-Re Π_{ij} model, their calculated difference is very substantial, even in the region away from the wall. When the normal heat flux is examined, large differences are also observed in the near-wall region of the model calculations. These discrepancies need further examination.

5. Further evidence of Reynolds-stress model sensitivity

The above results show that the Reynolds heat flux model is very sensitive to the near-wall Reynolds-stress models, but the two-equation heat flux model is not as sensitive. Since the model tested only differ in the near-wall corrections and in the wall reflection term, one could draw the conclusion that the discrepancies could be attributed to these differences. In order to further verify whether the near-wall corrections and the wall reflection term are indeed the cause, the HL, LSH and SAYS models were used to calculate the Kader (1981) case using the same two-equation and Reynolds heat flux models. The results, shown in Figs. 1–6, are compared with data and the previous predictions. These three models differ in several ways compared to the two models examined above. For example, among the five models considered, the HL model is independent of geometry, while the SAYS model assumes a different Π_{ij} model. On the other hand, the LSH model accounts for near-wall anisotropy through Π_{ij} modeling rather than by

modifying ε_{ij}. Therefore, these additional results could illustrate the effects, if any, of geometry dependence, and Π_{ij} and ε_{ij} modeling.

It would be prudent to first examine the two-equation heat flux model in order to assess the general validity of the above conclusion concerning the LS and ZSZ models. The U^+ results of the five models are compared in Fig. 1. It can be seen that all five models are able to reproduce the log law but they give different intercepts. Three models (LSZ, ZSZ and SAYS) yield an intercept of about 5, while the HL model gives a value of about 5.5 and the LS model a value of ~ 4.0. In terms of the asymptote $k^+/\varepsilon^+ y^{+2}$, two models (ZSZ and SAYS) give 0.5, two models (LSH and LS) yield 0.48, while one model (HL) predicts 0.41. As can be seen in Fig. 2, the differences in the near-wall asymptotes greatly affect the prediction of Θ^+. The LS, ZSZ and SAYS model predictions do not seem to be affected by the incorrect calculations of U^+ away from the wall, while those of HL and LSH are affected to different degrees by the mean flow calculations. These results are consistent with the predictions of $v\theta^+$, θ^{+2} and ε_θ^+ shown in Figs. 3–5. The HL model under-estimates $v\theta^+$ and θ^{+2} across the whole pipe and gives a far higher error in the estimate of ε_θ^+ in the near-wall region. According to (9), α_t depends to a great extent on the ratios k^+/ε^+ and $\theta^{+2}/\varepsilon_\theta^+$, therefore, an incorrect estimate of $\theta^{+2}/\varepsilon_\theta^+$ could lead to substantial errors in the prediction of $v\theta^+$ and hence Θ^+. A comparison of the near-wall asymptotes, $k^+/\varepsilon^+ y^{+2}$ and $\theta^{+2}/\varepsilon_\theta^+ y^{+2}$, between three model predictions is given in Fig. 7. The ZSZ and SAYS model results are not shown because they are essentially the same as those given by the LS model. It is obvious that the HL model predictions are not asymptotically consistent near a wall. Therefore, if the Reynolds-stress model is not asymptotically consistent in the near-wall region, it could greatly affect the prediction of the thermal field even when the heat flux model is one level lower than the velocity field model.

Even though the Θ^+ results deduced from the SAYS model using a two-equation heat flux model are in agreement with Kader's data, its prediction of Θ^+ using a Reynolds heat flux model is the worst among the five Reynolds-stress models considered (Fig. 6). It cannot even reproduce the buffer region correctly. The HL model, which gives a poor prediction in the two-equation case, manages to mimick the data all the way to $y^+ = 25$. This compares with an agreement up to $y^+ = 5$ only for the SAYS and ZSZ model. This shows that the modeled Reynolds heat flux equation is not just sensitive to the pressure strain model and/or the wall reflection term, but is also very sensitive to the modeled Reynolds-stress equation as a whole. In order to further identify the cause of these discrepancies, the LS and ZSZ models and the Reynolds heat flux model were used to calculate other cases for analysis.

Since Lai and So (1990a) showed good agreement with data in their calculations of the pipe flow experiment of Johnk and Hanratty (1962), this case is again examined using the LS and ZSZ models and the Reynolds heat flux model. The Θ^+ and $v\theta^+$ results are shown in Figs. 8 and 9. Consistent with the results shown in Fig. 6, there is a large difference between the model predictions. The ZSZ model under-predicts Θ^+ substantially over the whole pipe except in the viscous sublayer region (Fig. 8). Specifically, if the log layer is approximated by

$$\Theta^+ = \frac{1}{\kappa_\theta} \ln y^+ + B_\theta \tag{25}$$

the thermal von Karman constant, κ_θ, is predicted approximately correctly, but the calculated constant B_θ shows a very large error. It seems that the ZSZ model yields an excessively large friction temperature, Θ_τ. The reason for this error could be partially attributed to the calculation of $v\theta^+$. It can be seen

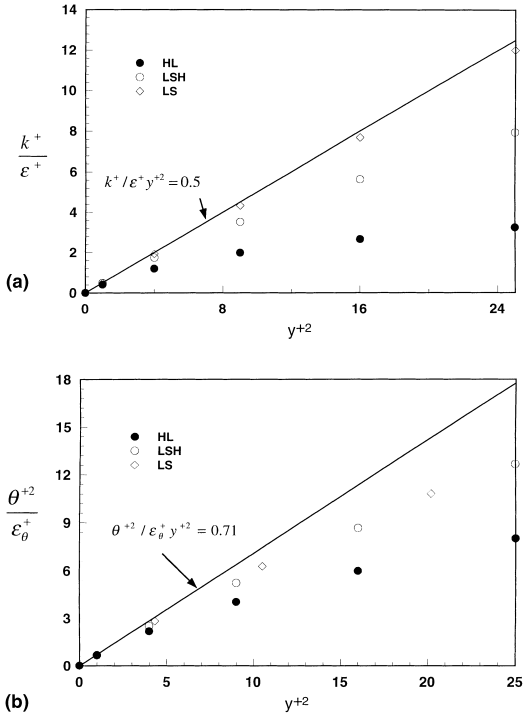

Fig. 7. Comparisons of the near-wall asymptotes as predicted by the HL, LS and LSH models.

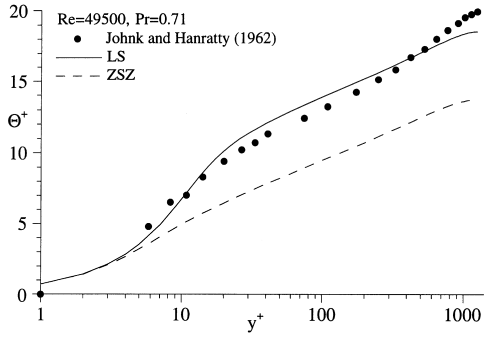

Fig. 8. Comparisons of Θ^+ calculations using a Reynolds heat flux model and two different Reynolds-stress models with data.

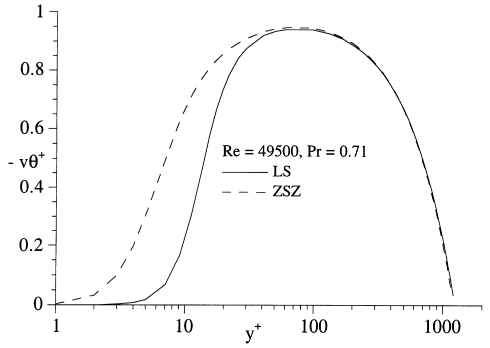

Fig. 9. Comparisons of $v\theta^+$ calculations using a Reynolds heat flux model and two different Reynolds-stress models.

that there is a large difference in the predicted $v\theta^+$ in the near-wall region (Fig. 9); up to $y^+ = 50$, the ZSZ model gives rise to a much larger heat flux than that of the LS model. This performance is rather baffling, especially when the only difference between the two models is in the wall reflection term and in ξ.

Similar results are also observed for a fully-developed channel flow with a much lower $Re = 4560$ but the same $Pr = 0.71$. Comparisons are made with the direct numerical simulation (DNS) channel flow data of Kasagi et al. (1992). The mean velocity results are compared in Fig. 10, the mean temperature profiles in Fig. 11 and the normal heat flux distributions in Fig. 12. Again, the results obtained from the LS model are in good agreement with DNS data, while those deduced from the ZSZ model are not. In particular, there is good agreement between the DNS data for $v\theta^+$ and the LS model prediction across the whole channel. As before, the ZSZ model over-predicts $v\theta^+$ in the near-wall region.

The discrepancies cannot be explained by differences noted in the prediction of U^+ alone. For example, the ZSZ model over-predicts U^+ for the DNS case (Fig. 10) and gives a correct U^+ distribution in the Kader case (Fig. 1). However, it yields a slightly better prediction of Θ^+ for the DNS case (compared Figs. 6 and 12). Although U^+ differs by about 10% between the LS and ZSZ model, the calculated Θ^+ differs by 30% or more. Therefore, influences other than the direct effect of the difference in U^+ have to produce this disproportionate discrepancy. This observation is also true for the HL, LSH and SAYS models.

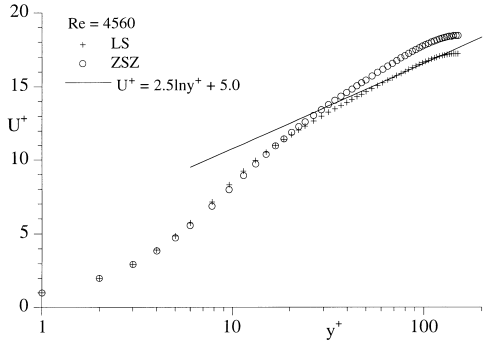

Fig. 10. Comparisons of mean velocity calculations using a Reynolds heat flux model and two different Reynolds-stress models with the log law.

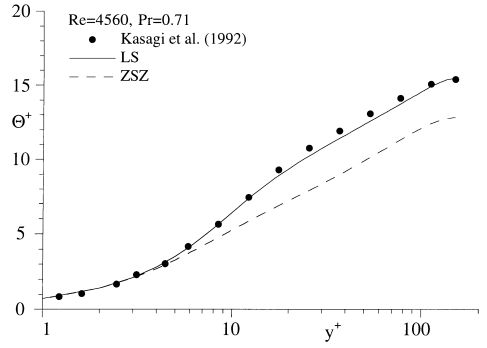

Fig. 11. Comparisons of Θ^+ calculations using a Reynolds heat flux model and two different Reynolds-stress models with data.

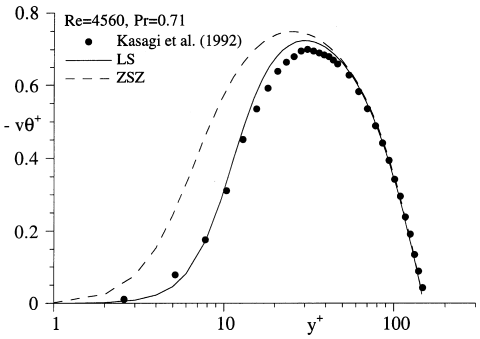

Fig. 12. Comparisons of $v\theta^+$ calculations using a Reynolds heat flux model and two different Reynolds-stress models with data.

6. Error analysis

An attempt is now made to identify the source of this error. Since the LS and ZSZ models are very similar, an error analysis conducted on these two model calculations could be most enlightening. Obviously, one could try to attribute this error to numerical integration. However, the equations solved are ordinary differential equations and the Newton iteration scheme used to integrate them is well established with known truncation errors. Since the percentage error noted is not the same for the two Reynolds-stress models, it cannot be due to numerical error alone. In view of this, the most likely error source is the modeled equations; either from the calculated Reynolds stresses or from the Reynolds heat fluxes. Further, the same sets of Reynolds-stress equations are used to calculate the turbulent thermal field using a near-wall two-equation heat flux model and yield little or no errors in the prediction of the mean temperature. Therefore, the source of error associated with the mean temperature is most likely derived from the modeled heat flux equation. This section attempts to identify the modeled terms that are responsible for the large error and to analyze their sensitivity. However, before attempting to do so, the consistency of the predicted $v\theta^+$ and Θ^+ needs to be assessed because, in a fully developed pipe and channel flow, the equation for $v\theta^+$ only depends on Θ^+.

At first sight, the large error incurred in the calculation of Θ^+ (Fig. 8) might not appear to be consistent with that shown in the calculated $v\theta^+$ (Fig. 9). In order to show that the errors are indeed consistent, the equation for Θ^+ has to be re-examined. For simplicity, the case of a fully developed channel flow, such as that shown in Figs. 10–12 is given below. In non-dimensional form, the Θ^+ equation can be written as

$$\frac{1}{Pr}\frac{\partial \Theta^+}{\partial y^+} = 1 - \left(\int_0^{y^+} U^+(\eta)\,\mathrm{d}\eta \Big/ \int_0^{Re_\tau} U^+(\eta)\,\mathrm{d}\eta \right) + v\theta^+ \qquad (26)$$

for the case of a flow with a constant wall heat flux, and

$$\frac{1}{Pr}\frac{\partial \Theta^+}{\partial y^+} = \frac{Re_\tau - y^+}{Re_\tau} + v\theta^+ \qquad (27)$$

for a flow with either a constant wall temperature or a constant internal heat source. Here, Re_τ is actually y^+ evaluated at the centerline of the channel. Integrating (26) or (27), the contribution of the heat flux term is given by the area beneath the curve representing $-v\theta^+$ in Fig. 12. How, then, could such a seemingly small difference in the area contribute to a large error in the calculated mean temperature? The reason is that the total contribution of the right-hand side of (26) or (27)

represents the difference of two large areas. It can also be seen that for the case of a constant wall temperature with a constant internal source, the mean velocity does not directly enter into the Θ^+ equation. As for the constant wall heat flux case, the direct effect of the mean velocity should be small, at least as long as the shape of the velocity profile is predicted fairly correctly. An error in the magnitude of the mean or center line velocity would affect both the numerator and the denominator in (26) equally. Thus, the error has to be introduced through the prediction of $v\theta^+$.

In order to demonstrate this point more clearly, the heat flux near the wall is approximated by the Taylor series expansion

$$-v\theta^+ = a_{v\theta}y^{+3} + b_{v\theta}y^{+4} + \cdots \tag{28}$$

Using only the leading term of (28) to approximate the heat flux up to $y^+ \approx 8$, the difference in Θ^+ due to the difference in $a_{v\theta}$ can be estimated. This approximation is legitimate since the results of Sommer et al. (1992) show that $-v\theta^+$ is very well approximated by the leading term of (28) in the viscous sublayer and even at $y^+ \approx 8$, the error incurred by neglecting the higher order terms is fairly small. Besides, only an estimate is sought here. The different values calculated in this manner are summarized in Table 1. It can be seen that the difference due to the leading coefficient is estimated in the right direction, i.e. the results obtained using the ZSZ model have a lower mean temperature than those deduced from the LS model. Also, comparison of Figs. 11 and 12 shows that the estimated ΔT^* in Table 1 agree well with the difference of the model calculations at the same location. Thus, it can be concluded that the solution of (26) is consistent with the normal heat flux obtained. In other words, the errors are most likely due to a wrong prediction of $-v\theta^+$.

Having traced the difference in the calculated results to the $v\theta^+$ equation, it is now necessary to ascertain that the difference observed in $v\theta^+$ is consistent with the equation solved. This could be accomplished by re-analyzing the equations for $v\theta^+$ and Θ^+. For simplicity, the constant wall temperature case, or (27), is investigated here. Furthermore, it was noted by Kasagi et al. (1992) that the mean temperature profiles for the two thermal boundary conditions are essentially identical. Therefore, the conclusions derived from the analysis of (27) could also be extended to (26). Differentiating (27) with respect to y yields

$$\frac{\partial v\theta^+}{\partial y^+} = \frac{1}{Pr}\frac{\partial^2\Theta^+}{\partial y^{+2}} + \frac{1}{Re_\tau}. \tag{29}$$

From (4), the modeled equation for $v\theta^+$ can be simplified to

$$\frac{\partial}{\partial y^+}\left[\left(\frac{2+Pr^{-1}}{3} + 2C_s\frac{k^+}{\varepsilon^+}v^{+2}\right)\frac{\partial v\theta^+}{\partial y^+}\right] - v^{+2}\frac{\partial\Theta^+}{\partial y^+} - \left[C_{1\theta}(1-f_{w\theta}) + f_{w\theta}(2+Pr^{-1})\right]\frac{\varepsilon^+}{k^+}v\theta^+ = 0. \tag{30}$$

Substituting (27) and (29) into (30) yields an equation for Θ^+. Noting that $f_{w\theta} = 1$ can be assumed in the immediate vicinity of the wall, the equation thus obtained for Θ^+ becomes

$$\frac{2+Pr^{-1}}{3Pr}\frac{\partial^3\Theta^+}{\partial y^{+3}} - (2+Pr^{-1})\frac{\varepsilon^+}{k^+}\left[\frac{1}{Pr}\frac{\partial\Theta^+}{\partial y^+} + \frac{y^+}{Re_\tau} - 1\right] = 0. \tag{31}$$

Eq. (31) is valid to order y^{+2} in the near-wall region. This equation contains coefficients that are either constant or depend on the velocity field only. Assuming Taylor series expansions for Θ^+, k^+, v^{+2} and ε^+, it can be shown that

$$\Theta^+ = A_\theta y^+ + B_\theta y^{+2} + C_\theta y^{+3} + \cdots, \tag{32a}$$

$$k^+ = a_k y^{+2} + b_k y^{+3} + \cdots, \tag{32b}$$

$$v^{+2} = a_{v^2}y^{+4} + b_{v^2}y^{+5} + \cdots, \tag{32c}$$

$$\varepsilon^+ = a_\varepsilon + b_\varepsilon y^+ + c_\varepsilon y^{+2} + \cdots \tag{32d}$$

Terms that are important near the wall can be easily determined. It can be seen that only ε^+/k^+ appears in (31). An expansion for the ratio ε^+/k^+ can be written as

$$\frac{\varepsilon^+}{k^+} = \frac{a_{\varepsilon k}}{y^{+2}} + \frac{b_{\varepsilon k}}{y^+} + c_{\varepsilon k} + d_{\varepsilon k}y^+ + \cdots \tag{33}$$

According to So et al. (1991), the coefficient $a_{\varepsilon k}$ has an asymptotic value of 2. This is recovered by the LS and ZSZ models considered. As for the remaining coefficients, they are different for different models and will be determined from the model calculations later. The reason for the use of (33) is that these coefficients can be determined more accurately than the coefficients of the individual expansions (32a)–(32d).

The equations to be balanced for each order are:

$$\frac{1}{Pr}A_\theta - 1 = 0, \quad \mathrm{O}\left(\frac{1}{y^{+2}}\right), \tag{34}$$

$$\frac{1}{Re_\tau} + \frac{2}{Pr}B_\theta + \frac{b_{\varepsilon k}}{a_{\varepsilon k}}\left[\frac{1}{Pr}A_\theta - 1\right] = 0, \quad \mathrm{O}\left(\frac{1}{y^+}\right), \tag{35}$$

$$3C_\theta + \frac{b_{\varepsilon k}}{a_{\varepsilon k}}\left[\frac{1}{Re_\tau} + \frac{2}{Pr}B_\theta\right] + \frac{c_{\varepsilon k}}{a_{\varepsilon k}}\left[\frac{1}{Pr}A_\theta - 1\right] = 0, \quad \mathrm{O}(y^{+^\circ}), \tag{36}$$

while the terms for higher orders are too complicated to be useful for the present analysis. If all orders can be solved exactly, it can be seen that the solutions will lead to $A_\theta = Pr$, as noted by Kim and Moin (1989), Antonia and Kim (1991) and others. The other solutions will give $B_\theta = -PrRe_\tau/2$ and $C_\theta = 0$. Note that up to this order, the results are independent of the coefficients of (33) and therefore, independent of the model used to calculate the velocity field. Thus, the exact solution shows that the third-order term in (32a) vanishes.

Table 1
Estimated error in Θ^+ at $y^+ \approx 8$ due to the LS and ZSZ models

Re	Near-wall Reynolds-stress models	$a_{v\theta} \times 10^3$	$T^* = Pr\int_0^8 a_{v\theta}\eta^3\,\mathrm{d}\eta$	ΔT^*
4560	LS	0.22	−0.16	–
	ZSZ	2.50	−1.82	−1.66
40,000	LS	0.15	−0.11	–
	ZSZ	3.00	−2.18	−2.07

However, when the transport Eq. (30) is solved numerically, it is not possible to obtain exact solution to (34). Consequently, (35) and (36) would not lead to the solutions $B_\theta = -PrRe_\tau/2$ and $C_\theta = 0$ and the predicted Θ^+ would be in error near the wall. A small numerical error could be introduced in the leading term of Θ^+. This error could be of a magnitude so small, that the error on this term itself would be fully acceptable, if it would not propagate to higher order terms. Assuming that a small error occurs in the calculation of A_θ, one could then try to determine the magnitude of the errors in B_θ, C_θ, and so on. Solving (35) for B_θ and (36) for C_θ, the following expressions are obtained:

$$B_\theta = \frac{Pr}{2}\left[\frac{b_{\varepsilon k}}{a_{\varepsilon k}}\left(1-\frac{1}{Pr}A_\theta\right)-\frac{1}{Re_\tau}\right], \tag{37}$$

$$C_\theta = \frac{1}{3}\left[\frac{c_{\varepsilon k}}{a_{\varepsilon k}}\left(1-\frac{1}{Pr}A_\theta\right)+\frac{b_{\varepsilon k}}{a_{\varepsilon k}}\left(\frac{1}{Re_\tau}+\frac{2}{Pr}B_\theta\right)\right]. \tag{38}$$

These two relations can be solved, if values for the coefficients in (33) are determined from the velocity field calculated using the near-wall Reynolds-stress models, while A_θ is estimated from the results shown in Figs. 10–12. For the two cases presented in Table 1, the results are summarized in Table 2. It can be seen that while the error in A_θ is very small and could be tolerated, the error in the next coefficient, B_θ, is much larger. Consistent with the results discussed above, the error is much larger in the case of the ZSZ model. Also, the errors show a deviation from the exact result which is consistent with the results obtained from model calculations. It is not possible to determine $c_{\varepsilon k}$, $d_{\varepsilon k}$, and so on, with any degree of accuracy. Thus, it cannot be shown here that the error in the mean temperature is consistent with the series solution to higher order than those examined above. In view of these analyses, it could be hypothesized that the modeled near-wall Reynolds heat flux equation is very sensitive to the modeled near-wall Reynolds-stress equation.

Another observation could be made from this analysis. Part of the reason why the calculated Θ^+ is so sensitive to the leading coefficients, $a_{\varepsilon k}$ and $b_{\varepsilon k}$, in (33) could be due to the assumption made in the modeling of the pressure scrambling term. According to the model proposed in (3) for $\Phi_{i\theta}$, only the velocity time scale, k/ε, has been used. However, Launder (1978) suggested that both k/ε and the thermal time scale, $\theta^2/\varepsilon_\theta$, should be taken into account in the modeling of the $\Phi_{i\theta}$ term. In other words, if the Reynolds heat flux model is to be made less sensitive to $a_{\varepsilon k}$ and $b_{\varepsilon k}$, the modeling of $\Phi_{i\theta}$ has to include a term with $\theta^2/\varepsilon_\theta$ explicitly specified and two more transport equations for θ^2 and ε_θ have to be solved, even for incompressible flows with heat transfer. Whether this latter approach, which involves solving two more equations, proves to be less sensitive to $a_{\varepsilon k}$ and $b_{\varepsilon k}$ remains to be verified.

When a two-equation heat flux model is used, $\overline{u_i\theta}$ is given by (8) and α_t is given by (9). If similar expansions are assumed for θ^{+2} and ε_θ^+ such that

$$\theta^{+2} = a_\theta y^{+2} + b_\theta y^{+3} + c_\theta y^{+4} + \cdots, \tag{39a}$$

$$\varepsilon_\theta^+ = a_\varepsilon\theta + b_{\varepsilon\theta} y^+ + c_{\varepsilon\theta} y^{+2} + \cdots, \tag{39b}$$

it can be shown that the leading coefficient of $v\theta^+$ is $(a_k^{3/4}a_\theta^{1/2})/(a_{\varepsilon\theta}^{1/2}a_{\varepsilon k}^{1/4})$. This term depends on $a_{\varepsilon k}$, which is 2 and is determined correctly by all near-wall Reynolds-stress models considered here. It also depends on a_k, a_θ and $a_{\varepsilon\theta}$, though. These coefficients are calculated with fair accuracy by the LS, ZSZ, LSH and SAYS models in conjunction with a two-equation heat flux model. Consequently, the calculated thermal field is much less sensitive to these models. This is not true for the HL model, because it is known to give incorrect estimates for a_k, a_θ and $a_{\varepsilon\theta}$. For example, the a_k deduced from the HL model is less than 50% of that calculated from the LS model in the case of fully-developed channel flow (So et al., 1991). This is a substantial difference and could be the cause of the discrepancy shown in Fig. 2.

7. An alternative to Reynolds heat flux model

It is now clear that the solution of the modelled $v\theta^+$ equation is very sensitive to the prediction of the coefficients in the expansion (33). All near-wall Reynolds-stress models are known to yield the first coefficient $a_{\varepsilon k}$ correctly (So et al., 1991). However, their predictions of the other coefficients differ widely. At this point, it is not at all clear whether it is possible to formulate two Reynolds-stress models that could give identical coefficients for (33) and/or a Reynolds heat flux model that is relatively insensitive to these coefficients. The advantage of a Reynolds heat flux model over that of a two-equation model is its ability to give a reasonable prediction of the streamwise heat flux which may be important for complex flow with heat transfer (Launder, 1978; Lai and So, 1990a). Of course, such is not possible with a two-equation model because, according to (8), the streamwise heat flux is a function of the streamwise mean temperature gradient alone. In other words, (8) fails to model the generation of a streamwise heat flux due to the interaction of the turbulent eddies with the mean temperature gradient normal to the wall. If an algebraic heat flux model that gives an estimate of the streamwise heat flux comparable to that predicted by the Reynolds heat flux model, and is based on the solution of (5)–(10), can be formulated, sensitivity of the thermal field calculations to the near-wall Reynolds-stress models could be reduced. Such a model would be a viable alternative to the Reynolds heat flux model.

One such model has recently been formulated by So and Sommer (1996). It is an explicit algebraic heat flux (EAHF) model. Usually, algebraic models derived in a straightforward manner are implicit and singular behavior could arise as a result of the mean strain approaching zero in the flow field. So and Sommer (1996) derived their model following the approach of Gatski and Speziale (1993) to avoid singular behavior inherent in any implicit algebraic model. The starting point of their analysis is (4) minus the near-wall correction

Table 2
Near-wall coefficients and errors in the estimate of A_θ and B_θ

Re	Near-wall Reynolds-stress models	$a_{\varepsilon k}$	$b_{\varepsilon k}$	A_θ	Error in A_θ (%)	$B_\theta \times 10^3$	Error in B_θ (%)
4560	LS	2.0	0.088	0.7099	0.014	−2.364	0.09
	ZSZ	2.0	−0.080	0.7091	0.127	−2.546	7.61
40,000	LS	2.0	0.094	0.7099	0.014	−0.335	0.69
	ZSZ	2.0	−0.115	0.7089	0.155	−0.369	9.37

terms. Equilibrium turbulence is invoked to simplify the equation to an algebraic equation in $\overline{u_i\theta}$. The equation thus deduced is not explicit for $\overline{u_i\theta}$ and singular behavior of the matrix could result for certain combination of the mean strain tensor and mean temperature gradient vector. A successive approximation technique is used to render the equation explicit for $\overline{u_i\theta}$. This involves postulating gradient transport models for the Reynolds stresses and heat fluxes that are associated with the mean gradient terms in (4). The model assumed for the Reynolds stresses is given by $\overline{u_iu_j} = (2/3)\delta_{ij}k - 2\nu_t S_{ij}$ where $\nu_t = C_\mu f_\mu(k^2/\varepsilon)$ is the eddy viscosity defined with respect to k and $\varepsilon, f_\mu = (1 + 3.45Re_t^{-1/2})\tanh(y^+/115)$ and C_μ is a model constant taken to be 0.096. Again, (8) and (9) are used to model the heat flux vector. After much algebra, the final expression for $\overline{u_i\theta}$ can be written as

$$-\overline{u_i\theta} = \alpha_t\frac{\partial\Theta}{\partial x_i} - \frac{1}{C_{1\theta}}\sqrt{\frac{k}{\varepsilon}\frac{\overline{\theta^2}}{\varepsilon_\theta}}\{[2\nu_t + (1 - C_{2\theta})\alpha_t]S_{ik} + (1 - C_{2\theta})\alpha_t W_{ik}\}\frac{\partial\Theta}{\partial x_k}, \tag{40}$$

where $W_{ik} = (1/2)[\partial U_i/\partial x_k - \partial U_k/\partial x_i]$ is the mean rotation rate tensor. In view of this modification to (4) and in order that (40) would recover correctly the result deduced from (8) for fully developed pipe and channel flows, the model constants in (40) have to take on values given by $C_{1\theta} = 3.28$ and $C_{2\theta} = 0.4$, while α_t is still given by (9). It can be seen from (40) that the second term is non-zero even when the stream wise mean temperature gradient is zero and it allows the modeling of the generation of a streamwise heat flux due to the interaction of the turbulent eddies with the mean temperature gradient normal to the stream direction.

This model still relies on the solution of Eqs. (5)–(10). Since the modeled equations solved are the same as those in two-equation model and according to (40), the contribution of the second term to the normal heat flux is essentially negligible, the effect of near-wall Reynolds-stress models on the thermal field calculation could be reduced to a minimum. Therefore, the EAHF model only improves the prediction of the streamwise heat flux. So and Sommer (1996) have validated the EAHF model for a number of flows with different Re, so there is no need to repeat their results here. However, one sample calculation to illustrate that the calculated thermal field is not affected by the near-wall Reynolds-stress models will be shown together with the improved prediction of the streamwise heat flux. Since the experiment of (Hishida et al., 1986) provides $\overline{u\theta}$ measurements at $Re = 40,000$ and $Pr = 0.71$, the EAHF model is used in conjunction with the LS model and the two-equation heat flux model to calculate this case and compared with the calculations presented in Figs. 1–5. Only the calculated streamwise heat flux (Fig. 13) is shown because all other results are the same as before (Figs. 1–5). As expected, the EAHF model greatly improves the prediction of $u\theta^+ = \overline{u\theta}/u_\tau\Theta_\tau$ (Fig. 13). For fully-developed channel flow, $u\theta^+$ predicted by (8) is essentially zero across the channel because $\partial\Theta/\partial x$ is extremely small.

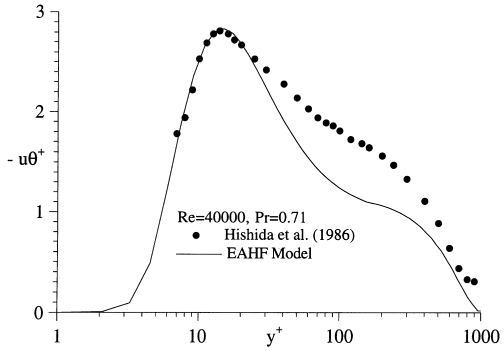

Fig. 13. Comparison of the calculated $u\theta^+$ using the EAHF model with data.

8. Conclusions

The effects of five different near-wall Reynolds-stress models on the calculated thermal field in an incompressible flow are investigated. It is found that the calculated mean temperature is very sensitive to the near-wall Reynolds-stress model used to evaluate the velocity field. The sensitivity is traced to the near-wall asymptotes, k^+/ε^+y^{+2}, $\theta^{+2}/\varepsilon_\theta^+y^{+2}$, a_k, a_θ and $a_{\varepsilon\theta}$, in the case of the two-equation heat flux model and to the modeled equation for the normal heat flux in the case of the Reynolds heat flux model. Incorrect prediction of these asymptotes could lead to an erroneous estimate of the normal heat flux and hence the mean temperature. As for the Reynolds heat flux model, an error analysis has been carried out to examine the modeled equations near a wall. In this case, the normal heat flux and the mean temperature equations were used to derive an equation for the mean temperature. The resultant equation was found to depend on the coefficients of the asymptotic expansions for Θ^+ and ε^+/k^+ near a wall. The first coefficients in these expansions were estimated correctly by the LS and ZSZ models considered. However, their estimates of the second- and higher-order coefficients differed greatly from each other. Since error in the lower coefficient propagates to give rise to greater error in the higher-order coefficients, the integration gives rise to substantial error to the predicted mean temperature. The formulation of near-wall Reynolds- stress models that could yield correct coefficients for the ε^+/k^+ expansion up to y^{+2} or higher may not be possible at present. Therefore, it would be better to calculate the turbulent thermal field using a heat flux model that is one level lower than the velocity field model. Even then, there is no guarantee that the thermal field could be calculated correctly, unless the Reynolds-stress model adopted could yield the correct near-wall asymptotes. Under these conditions, an explicit algebraic heat flux EAHF model, which is based on the solution of the equations governing the transport of the temperature variance and its dissipation rate, could be suggested as an alternative to the Reynolds heat flux model. This way, an estimate of the streamwise heat flux comparable to that given by the Reynolds heat flux model could be obtained. The EAHF model is shown to be independent of the LS and ZSZ model, because they can reproduce the near-wall behavior correctly.

Acknowledgements

Part of this work was carried out by RMCS and TPS during their tenure at Arizona State University. They wish to acknowledge support given to them by NASA Langley Research Center, Hampton, VA, under Grant No. NAG-1-1080. The Grant was monitored by Dr. T.B. Gatski. The work was completed by RMCS and CYZ at The Hong Kong Polytechnic University. They too wish to acknowledge the support given to them through Grant No. G-YW18.

References

Antonia, R.A., Kim, J., 1991. Turbulent Prandtl number in the near-wall region of a turbulent channel flow. International Journal of Heat and Mass Transfer 34, 1905–1908.

Cebeci, T., Bradshaw, P., 1984. Physical and Computational Aspects of Convective Heat Transfer, Springer, New York, pp. 13, 19–31, 150–151.

Daly, B.J., Harlow, F.H., 1970. Transport equations in turbulence. The Physics of Fluids 13, 2634–2649.

Gatski, T.B., Speziale, C.G., 1993. On explicit algebraic stress models for complex turbulent flows. Journal of Fluid Mechanics 254, 59–78.

Hanjalic, K., Launder, B.E., 1972. A Reynolds-stress model of turbulence and its application to thin shear flows. Journal of Fluid Mechanics 52, 609–638.

Hanjalic, K., Launder, B.E., 1976. Contributions towards a Reynolds-stress closure for low-Reynolds-number turbulence. Journal of Fluid Mechanics 74, 593–610.

Hishida, M., Nagano, Y., Tagawa, M., 1986. Transport processes of heat and momentum in the wall region of turbulent pipe flow. Proceedings of the Eighth International Heat Transfer Conference 3, 925–930.

Johnk, R.E., Hanratty, T.J., 1962. Temperature profiles for turbulent flow of air in a pipe-I the fully developed heat transfer region. Chemical Engineering Sciences 17, 867–879.

Kader, B.A., 1981. Temperature and concentration profiles in fully turbulent boundary layers. International Journal of Heat and Mass Transfer 24, 1541–1544.

Kasagi, N., Tomita, Y., Kuroda, A., 1992. Direct numerical simulation of the passive scalar field in a turbulent channel flow. Journal of Heat Transfer 114, 598–606.

Kim, J., Moin, P., 1989. Transport of Passive Scalars in a Turbulent Channel Flow. Turbulent Shear Flows 6, Springer, Berlin, pp. 85–96.

Kolmogorov, A.N., 1941. Local structure of turbulence in incompressible viscous fluids for very large Reynolds number. Doklady AN SSSR 30, 299–303.

Lai, Y.G., So, R.M.C., 1990a. Near-wall modeling of turbulent heat fluxes. International Journal of Heat and Mass Transfer 33, 1429–1440.

Lai, Y.G., So, R.M.C., 1990b. On near-wall turbulent flow modeling. Journal of Fluid Mechanics 221, 641–773.

Launder, B.E., 1978. In: Bradshaw (Ed.), Heat and Mass Transport. Topics in Physics, vol. 12, Turbulence, Springer, New York, pp. 231–287.

Launder, B.E., Shima, N., 1989. Second-moment closure for the near-wall sublayer: development and application. AIAA Journal 27, 1319–1325.

Launder, B.E., Tselepidakis, D.P., 1993. Progress and paradoxes in modeling near-wall turbulence. Turbulent Shear Flows 8, 81–96.

Launder, B.E., Reece, G.J., Rodi, W., 1975. Progress in the development of a Reynolds stress turbulence closure. Journal of Fluid Mechanics 68, 537–566.

Nagano, Y., Shimada, M., 1996. Development of a two-equation heat transfer model based on direct simulations of turbulent flows with different Prandtl numbers. Physics of Fluids 8, 3379–3402.

Rotta, J.C., 1951. Statistiche Theroie Nichthomogener Turbulenz. Zeitschrift fur Physik 129, 547–572; 131, 51–77.

Shima, N., 1988. A Reynolds-stress model for near-wall and low-Reynolds-number regions. Journal of Fluids Engineering 110, 38–44.

Shir, C.C., 1973. A preliminary numerical study of atmospheric turbulent flows in the idealized planetary boundary layer. Journal of Atmospheric Science 30, 1327–1339.

So, R.M.C., Sommer, T.P., 1994. A near-wall Eddy conductivity model for fluids with different Prandtl numbers. Journal of Heat Transfer 116, 844–854.

So, R.M.C., Sommer, T.P., 1996. An explicit algebraic heat-flux model for the temperature field. International Journal of Heat and Mass Transfer 39, 455–465.

So, R.M.C., Yuan, S.P., 1999. A geometry independent near-wall Reynolds-stress closure. International Journal of Engineering Sciences 37, 33–57.

So, R.M.C., Yuan, S.P., Sommer, T.P., 1992. A hierarchy of near-wall closures for turbulent heat transfer. Trends in Heat, Mass and Momentum Transfer 2, 203–221.

So, R.M.C., Aksoy, H., Yuan, S.P., Sommer, T.P., 1996. Modeling Reynolds-number effects in wall-bounded turbulent flows. Journal of Fluids Engineering 118, 260–267.

So, R.M.C., Lai, Y.G., Zhang, H.S., Hwang, B.C., 1991. Second-order near-wall turbulence closures: a review. AIAA Journal 29, 1819–1835.

Sommer, T.P., So, R.M.C., 1996. Wall-bounded buoyant turbulent flow and its modeling. International Journal of Heat and Mass Transfer 39, 3595–3606.

Sommer, T.P., So, R.M.C., Lai, Y.G., 1992. A near-wall two-equation model for turbulent heat fluxes. International Journal of Heat and Mass Transfer 35, 3375–3387.

Sommer, T.P., So, R.M.C., Zhang, H.S., 1994. Heat transfer modeling and the assumption of zero wall temperature fluctuations. Journal of Heat Transfer 116, 855–863.

Speziale, C.G., So, R.M.C., 1998 Turbulence Modeling and Simulation. The Handbook of Fluid Dynamics, Richard W. Johnson (Eds.), CRC Press, Boca Raton, Florida, pp. 14.1–14.111.

Speziale, C.G., Sarkar, S., Gatski, T.B., 1991. Modeling the pressure-strain correlation of turbulence: an invariant dynamical systems approach. Journal of Fluid Mechanics 227, 245–272.

Zhang, H.S., So, R.M.C., Zhu, M.L., 1993. An asymptotically correct near-wall Reynolds-stress turbulence model. In: Proceedings of the Ninth Symposium on Turbulent Shear Flows, Kyoto, Japan, 16–18 August, Paper No. 8–2.